Pergamon

PII S0016-7037(01)00582-8

The solubility of rhenium in silicate melts: Implications for the geochemical properties of rhenium at high temperatures

W. Ertel,[1,†] H. St. C. O'Neill,[2,*] P. J Sylvester,[3] D. B. Dingwell,[1,‡] and B. Spettel[4]

[1]Bayerisches Geoinstitut, Universität Bayreuth, D 95440 Bayreuth, Germany
[2]Research School of Earth Sciences, Australian National University, Canberra, ACT 0200, Australia
[3]Dept. Earth Science, Memorial University of Newfoundland, St. John's, Newfoundland A1B 3X5, Canada
[4]Max Planck Institut für Chemie, D 55020 Mainz, Germany

Abstract—The solubility of rhenium (Re) in a haplobasaltic melt (anorthite-diopside eutectic composition) has been experimentally determined using the mechanically assisted equilibration technique at 1400°C as a function of oxygen fugacity ($10^{-12} < fO_2 \leq 10^{-7}$ bar), imposed by CO-CO_2 gas mixtures. Samples were analysed by laser ablation-inductively coupled plasma-mass spectrometry (LA-ICP-MS). This is a true microanalytical technique, which allows small-scale sample heterogeneity to be detected, while providing a limit of detection of 2 ppb Re. Time-resolved LA-ICP-MS spectra revealed the presence of suboptically sized micronuggets of Re in all samples, which, because they are present at the 0.5 to 10 ppm level, dominate the true solubilities of Re (<1 ppm at the conditions of the experiment) in bulk analyses of the samples. Nevertheless, the micronuggets could be filtered out from the time-resolved spectra to reveal accurate values of the true Re solubility. A number of time series of samples were taken at constant fO_2 to demonstrate that the solubilities converge to a constant value. In addition, solubilities were measured after increasing and decreasing the imposed fO_2. The results show that Re dissolves in the silicate melt as ReO_2 (Re^{4+}) and ReO_3 (Re^{6+}) species, with the latter predominating at typical terrestrial upper-mantle oxygen fugacities. The total solubility of Re is described by the following expression (fO_2 in bars):

$$[\text{Re/ppb}] = 9.7(\pm 1.9) \times 10^9 \, (fO_2) + 4.2 \, (\pm 0.3) \times 10^{14} \, (fO_2)^{1.5}$$

Assuming an activity coefficient for Re in Fe-rich metal of 1, this gives a value of $D_{Re}^{met/sil}$ of 5×10^{10} at log $fO_2 = $ IW-2, appropriate for metal-silicate partitioning in an homogenously accreting Earth. Thus, Re is indeed very highly siderophile, and the mantle's abundance cannot be explained by homogenous accretion. *Copyright © 2001 Elsevier Science Ltd*

1. INTRODUCTION

Rhenium (Re), together with the six platinum group elements (Ru, Rh, Pd, Ir, Os, and Pt) and Au, comprise a group of elements known as the highly siderophile elements (HSEs), the defining geochemical property of which is that they have metal-silicate distribution coefficients $D_M^{met/sil}$ in excess of 10^4. Their high metal-silicate distribution coefficients have resulted in their partitioning into the metal of the Earth's core. This, together with the fact that the HSEs are heavy elements with intrinsically low solar abundances, means that their abundances in the Earth's mantle are extremely low. In fact Re, with a bulk silicate Earth abundance of 0.2 ppb, is the rarest of all the naturally occurring elements, apart from the noble gases (e.g., O'Neill and Palme, 1999). Nevertheless, advances in geochemical analytical capabilities now enable the HSEs to be determined in a wide variety of igneous rocks. Interpretation of these analytical data requires some knowledge of the high-temperature geochemical properties of the HSEs, in particular

quantification of their metal-silicate and sulfide-silicate distribution coefficients.

In addition, identification of the valence states of Re in the high-temperature geological environment is a useful first step towards understanding the geochemical behaviour of this element. The common valence states of Re are 4+, 6+, and 7+, but previous experimental work (e.g., O'Neill et al., 1995; Righter and Drake, 1997) has suggested that Re dissolves in silicate melts as species with unusually low valence states (1+ or 2+). These low valence states are so rare that they are effectively unknown in solid state chemistry, and consequently, there is no indication of even the most fundamental chemical properties of Re in such states. However, these earlier experimental studies used bulk analytical methods. Some recent parallel studies on other HSEs raise the possibility that these earlier studies may have been compromised by the "micronugget effect" (O'Neill et al., 1995; Ertel et al., 1999), whereby the small amounts of Re chemically dissolved in the silicate melts may have been masked by larger amounts present as micronuggets. Micronuggets are submicroscopic particles, which seem to form something akin to a colloidal suspension. In this study we use a microanalytical technique, laser ablation-inductively coupled plasma-mass spectrometry (LA-ICP-MS), to see through the micronugget contamination and determine the true solubilities of Re in a haplobasaltic silicate melt (Anorthite-Diopside 1-atm eutectic composition). We demonstrate that the

*Author to whom correspondence should be addressed (hugh.oneill@anu.edu.au).
† *Present address:* Lunar and Planetary Laboratory, University of Arizona, Tucson, AZ 85721, USA.
‡ *Present address:* Institut für Mineralogie, Petrologie und Geochemie, Universität München, D 80333 München, Germany.
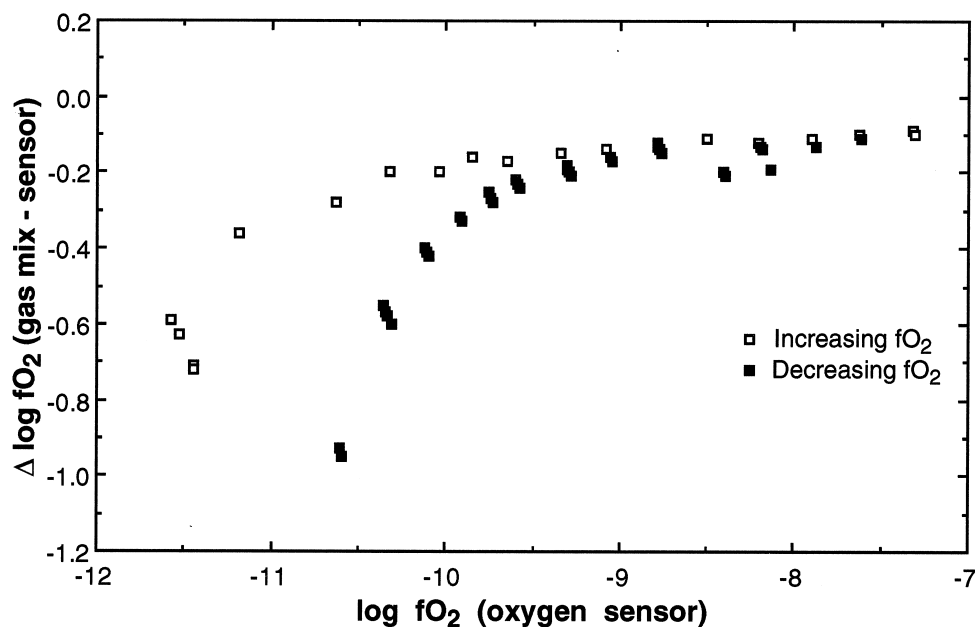
Fig. 1. Comparison of experimental oxygen fugacities calculated from CO-CO$_2$ gas-mixing ratios with those measured with a YSZ solid-electrolyte oxygen sensor (with air as the reference). At higher fO$_2$s many data overlap completely and are therefore not plotted. The development of two apparent curves at low fO$_2$ represents a small systematic difference between the beginning and the end of the experiment.

previous work was indeed in error from micronugget contamination. The valence states of dissolved Re in silicate melts are in fact the familiar 4+ and 6+. Micronuggets also probably affected previous experimental studies of Re metal-silicate partitioning, which are consequently biased to low values; the present results demonstrate unambiguously that Re is indeed an HSE with an enormous metal-silicate distribution coefficient at likely core-forming conditions.

2. EXPERIMENTAL

2.1. Sample Equilibration

Experiments were performed in a vertical tube furnace equipped for gas mixing, using the mechanically assisted equilibration technique of Dingwell et al. (1994). Oxygen fugacities were imposed using CO-CO$_2$ gas mixtures.

Starting silicate melt compositions were prepared by a gelling process (Hamilton and Henderson 1968) from Al metal powder, CaCO$_3$, MgO, and tetraethylorthosilicate (TEOS), to assure maximum homogeneity. The gel was fused in a Naber box furnace for 25 min in air in an Al$_2$O$_3$ crucible (Friatec, Friedrichsfeld). ~50 g of the resulting silicate melt (anorthite-diopside eutectic composition) was loaded into an Re crucible of 5 cm height and 1.5 cm diameter, and placed in the constant temperature zone in the middle of the furnace tube. The crucible was replenished with melt several times during the course of the experiment.

Because of the large volume of the crucible, an Re spindle continuously stirred the melt during the experiment to promote equilibration with the imposed gas mixture. The Re crucibles and spindle, which were designed specifically for this experiment, were obtained from Sandvik Rhenium Alloys Inc. (now Rhenium Alloys Inc.) of Elyria, Ohio, USA, and were stated to be of 99.9% purity.

The Re spindle originally consisted of a 20 cm long rod, with a spindle head of 1 cm diameter and 2 cm height. However, as detailed in O'Neill et al. (1995), the CO in the gas mixture attacks the Re stem near the top of the furnace, where the temperature is a few hundred centigrade, presumably forming Re carbonyl gas. The attack causes the

stem to be eaten through in a few days. To avoid this problem, the spindle stem was cut down and joined to stainless steel segments, which exit through an adjustable iris diaphragm at the top of the furnace. The spindle is attached to a rotary drive located immediately above the furnace. The motor speed could be electronically controlled and was set for this experiment at 60 rpm. A safety circuit checked the force on the spindle in case the spindle got stuck, in which case the power to the motor was cut to avoid damage.

Temperature was controlled via a type B (Pt$_{94}$ Rh$_6$/Pt$_{70}$Rh$_{30}$) thermocouple external to the alumina furnace tube, and was independently measured using a second type B thermocouple placed directly underneath the crucible. Temperature fluctuations were typically ±1°C over 24 h. Oxygen fugacity was imposed using CO-CO$_2$ mixtures, metered out by Tylan mass flow controllers. For both CO and CO$_2$, two mass flow controllers each were used with flow rate ranges of 0 to 10 and 0 to 200 SCCM, to control accurately mixtures at quite extreme ratios. In this way, the fO$_2$ at 1400°C was varied over five orders of magnitude, from 10^{-7} to 10^{-12} bars, corresponding to log fO$_2$ values relative to the iron-wüstite (or IW) oxygen buffer of −2.3 to +2.7 log-bar units. Oxygen fugacity was continuously monitored using an yttria-stabilized zirconia oxygen sensor (SIRO2, Eaglehawk, Australia), with air as reference. The EMF of the sensor was displayed on a high-impedance voltmeter and additionally recorded on a chart recorder. The values of fO$_2$ calculated from the sensor are compared to those calculated from the imposed CO : CO$_2$ ratios in Figure 1. At higher oxygen fugacities there is a small systematic difference in log fO$_2$ of ~0.15, but this increases to nearly 1 log-bar unit at very reducing conditions, where the CO : CO$_2$ ratio of the gas becomes large. There are two probable explanations for this. First, a small amount of O$_2$ may leak into the furnace where the stirring spindle exits through the iris diaphragm. This leak would be negligible at most experimental conditions, but becomes noticeable when the CO$_2$ content of the gas mixture is small (it is only 3.3% at the lowest fO$_2$ used in this study). Second, the YSZ sensor probably develops a significant component of electrical conductivity under these relatively reducing conditions (e.g., Mendybaev et al., 1998), resulting in lower EMFs than for true Nernstian behaviour. The problem of fO$_2$ accuracy at the lowest fO$_2$s can be left moot, since it turns out that the Re solubilities in this region are below our effective limit of detection anyway.

Samples were taken by removing the Re spindle and dipping a cold 3 mm diameter high-purity alumina rod into the melt. ~0.5 g of melt congealed around the rod, which was then quickly withdrawn and quenched into water. The quenching causes the congealed glass to shatter, making its recovery easy. A hazard of the technique in this particular experiment is the presence of volatile oxides or carbonyls of Re in the furnace, which may contaminate the exterior of the glass samples during withdrawal. Likewise, some Re was transported to the cooler parts of the furnace by these volatiles during the experiment, for example, to the top of the spindle or the iris diaphragm, where it condensed. Some of this Re occasionally flaked off during sampling. Under some conditions, a thin scum of Re formed on the surface of the melt in the Re crucible, perhaps from stray Re flakes of this condensed material dropping down into the crucible. All of these factors may contribute to possible contamination. Hence, the pieces of the quenched glass that were selected for further analysis were carefully examined to avoid any macroscopic Re contamination.

Experiments were performed according to two slightly different strategies. In an initial series of experiments undertaken to establish the feasibility of the experimental protocol, single samples were taken after sufficient time had elapsed for the Re concentration to reach steady state. A sufficient time was estimated from experience with similar experiments on other siderophile elements (Dingwell et al., 1994; Ertel et al., 1997, 1999). Obviously, it is somewhat unsatisfactory to rely on previous experience alone in this matter, and therefore, in a second, more detailed set of experiments, samples were taken in a time series at constant fO_2.

2.2. Analytical Methods

2.2.1. Major elements

The major element composition of samples was checked routinely during the experiment by electron microprobe analysis, using a CAMECA SX 50 at the Bayerisches Geoinstitut, University of Bayreuth, with wavelength dispersive spectrometry. Clear and microscopically clean glass chips were mounted in epoxy resin and polished. Raw data were reduced using the PAP correction program (Pouchou and Pichoir 1984). The standards used were wollastonite (Ca), enstatite (Mg), spinel (Al), and orthoclase (Si).

The melt composition for all samples was within analytical error of the target composition for the anorthite-diopside eutectic (10.8% MgO, 15.6% Al_2O_3, 50.3% SiO_2, and 23.8% CaO). It can be concluded that major element melt composition was not influenced or altered due to differing volatility of the melt components (e.g., SiO_2).

2.2.2. Instrumental neutron activation analyses (INAA)

The quenched glass samples were checked under an optical microscope for macroscopic contamination (e.g., black particles of Re oxide), and optically inclusion-free glass fragments, typically weighing between 30 and 80 mg each, were selected and sent to the Max Planck Institute for Cosmochemistry (Mainz, Germany) for INAA analyses. The irradiations were performed using the TRIGA-reactor of the Institut für Kernchemie at the Johannes Gutenberg Universität (Mainz, Germany). The neutron flux was 7×10^{11} n cm^{-2}s^{-1}, and the duration of the irradiation was 6 h. Samples were counted on large volume coaxial Ge(Li)-detectors.

For the Re analyses, the decay of ^{186}Re (137.2 keV, $T_{1/2}$ = 90.72 h) and ^{188}Re (155.0 keV, $T_{1/2}$ = 16.98 h) was registered. The detection limit of these analyses in 0.1 g of sample material is ~2 ppb. All samples were counted twice after 1 to 6 d with counting times of 10 to 30 min. Scandium activities (^{46}Sc, 889.2 keV and 1120.6 keV, $T_{1/2}$ = 93.843 d) were recorded simultaneously and used as an internal standard for INAA measurements.

2.2.3. Laser ablation-inductively coupled plasma-mass spectrometry (LA-ICP-MS)

Although INAA is suitable for quite small samples (e.g., here ~100 mg), LA-ICP-MS is a true microanalytical technique, which can resolve inhomogeneities on the scale of the material ablated by one laser pulse, that is, approximately 2 ng of sample (e.g., Ertel et al., 1999). This is important, as it is becoming widely recognised that most, if not all, experimental investigations of highly siderophile element (HSE) partitioning relationships involving silicate melts have been compromised by the presence of colloidal-sized micronuggets of the HSE in the melt.

LA-ICP-MS analyses were carried out at the Department of Earth Science, Memorial University of Newfoundland, using a Plasma Quad II Plus ICP-MS and a 1054 nm Nd-YAG laser, quadrupled to obtain a wavelength of 266 nm for better coupling to the silicate glass. The laser was pulsed at a frequency of 10 Hz, with an energy of 0.1 J per pulse. This resulted in nice ablation pits, with a sharp rim and no loss of energy due to crack formation.

NIST 612 glass containing 6.57 ppm Re (Sylvester and Eggins 1997) was used as a standard. This was checked against An-Di-eutectic glass samples containing Re that had previously been analysed by conventional sample-nebulization ICP-MS at the Research School of Earth Sciences, Australian National University, also using a Plasma Quad II Plus (see Ertel et al., 1999). Agreement was good, supporting the value of Re in the NIST 612 glass adopted here, although these An-Di-eutectic glasses showed somewhat greater inhomogeneity, possibly indicative of the presence of micronuggets. Since these latter samples are of identical major-element composition to the samples of this study, this check also shows that matrix effects are negligible. The internal standards were Si and Ca, while both ^{185}Re and ^{187}Re were determined during the analyses. ^{178}Hf and ^{179}Hf were determined simultaneously to check for potential ReO interferences. ^{189}Os count rates were trivial, indicating negligible interference of ^{187}Os on ^{187}Re (see Fig. 2).

The laser was kept firing continuously during the analytical session to ensure stability. The samples could be protected from the laser using the laser power meter as a shutter. This made quick changes between background and signal determination possible. Each measurement started with a background determination of ~60 s, after which the power meter was moved out of the laser beam, and the sample ablated. The laser beam was defocused to 150 μm above the sample surface using an optical microscope, resulting in a pit diameter of ~70 μm. Ablation was performed between 60 and 120 s, depending on the stability of the signal. If the ablation signal indicated the presence of micronuggets, the longer time (120 s) was used. Each block of measurements consisted of twice measuring the standard glass (NIST 612), and then a maximum of 16 samples before the standard was remeasured to determine any drift. Data were recorded as time-resolved spectra (counts per s versus time).

Examples of time-resolved spectra are shown in Figure 2. Micronuggets appear as hills, bumps, or spikes, amongst which the true Re solubility levels appear as flat-bottomed valleys. To obtain true Re solubilities, the integration limits were set with the aim of blocking out as much of the micronugget-based signal as possible. This becomes more difficult, the lower the level of Re in the sample relative to the micronugget contribution.

The limit of detection was estimated to be ~1.5 ppb from counting statistics. The presence of the micronuggets and possible memory effects associated with ablation of inhomogeneous samples suggest that the real limit of detection may be somewhat higher than this. In this study, we assume a limit of detection of 2 ppb, and samples which return lower apparent values are reported as <2 ppb (e.g., Table 2). The low limit of detection in the present study compares very well with that for Pt and Rh in a previous study (Ertel et al., 1999), in which the effective limit of detection was ~200 ppb due to the masking of any lower levels by micronuggets.

3. RESULTS

3.1. Re Solubilities

The experiment reported here lasted 7227 h (~10 months), during which 93 samples were taken at oxygen fugacities from 10^{-12} to $10^{-7.3}$ bars at 1400°C. All samples were analysed initially by INAA. Re concentrations were generally found to be in the range 0.5 to 10 ppm, with only a vague correlation with fO_2. Subsequently, the same samples were analysed by
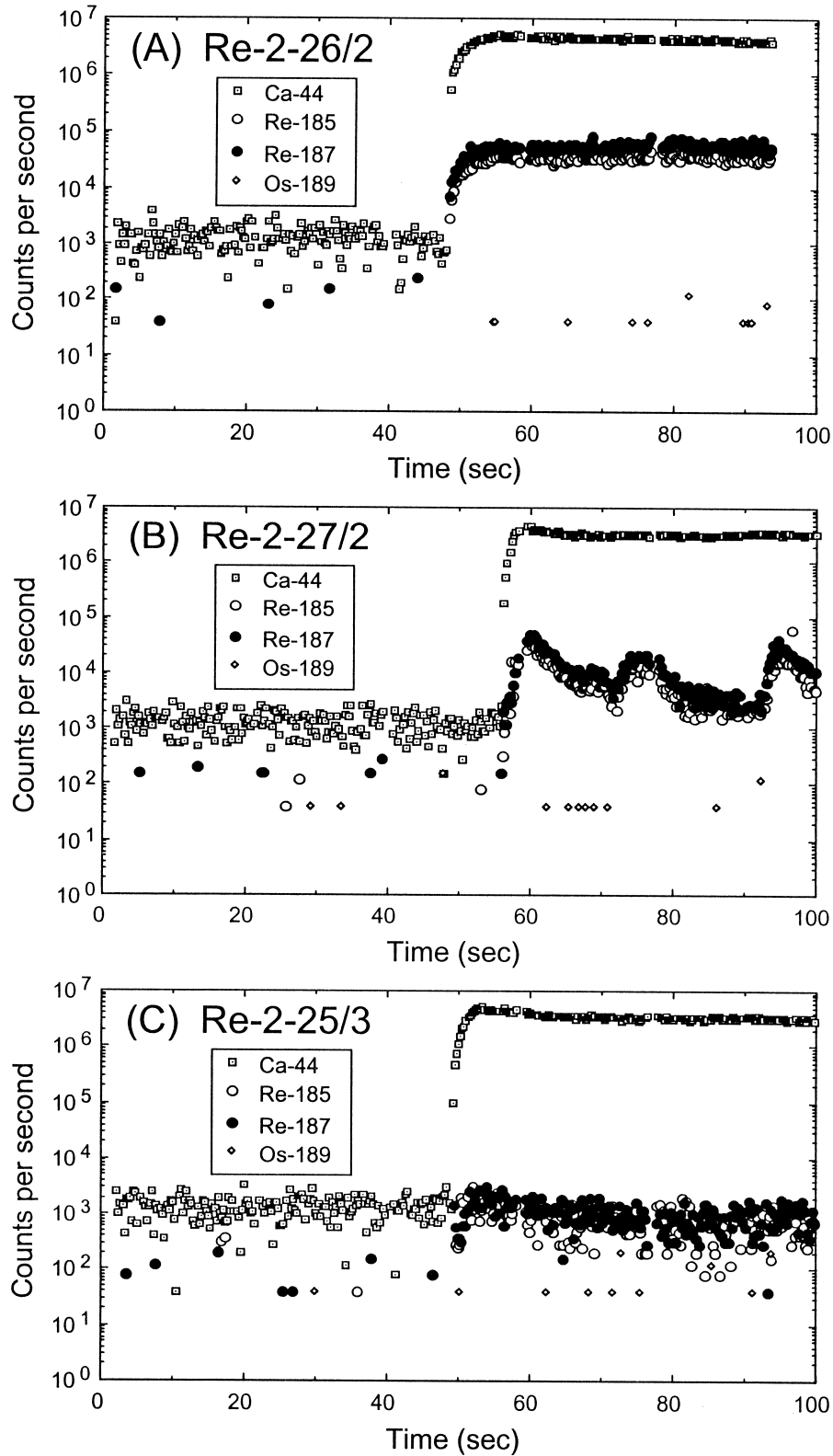
Fig. 2. Examples of time-resolved mass spectra from LA-ICP-MS analyses. (a) High dissolved Re levels (11 ppm). At this concentration the level of micronuggets is insignificant and the sample appears homogenous. (b) Severe micronugget contamination (5 ppm Re). (c) Medium levels of dissolved Re (300 ppb), homogenous.

Table 1. Single sample measurements. Each value is the mean of measurements from three spots.

Time (h)	Gas mix (CO:CO$_2$)	log fO$_2$[a]	Re (ppb)
789.3[b]	220:80	−9.34	13
96	200:100	−9.08	22
77.5	175:125	−8.78	46
94.5	150:150	−8.50	118
97	125:175	−8.20	290
119.5	100:200	−7.90	751
97.4	80:220	−7.63	1613
334.4	60:240	−7.31	5322
71.2	60:240	−7.31	5158
97	80:220	−7.62	1844
72.4	100:200	−7.88	815

[a] fO$_2$ in log-bar units, from the YSZ oxygen sensor. Values calculated from the CO-CO$_2$ gas mixture at 1400°C are ~0.15 log-bar units more reduced (see Fig. 1).

[b] Time from start of experiment. Includes steps from fO$_2$ = $10^{-11.5}$ bars to $10^{-9.34}$ bars, during which the Re concentration was continuously decreasing and a steady state was not reached. Initial Re concentration was ~3000 ppb (see Fig. 3a).

LA-ICP-MS. The latter method is a true microanalytical technique, since each ablation pulse removes material with diameter 70 μm to a depth of 0.2 μm, that is, ~2 ng. The LA-ICP-MS analyses revealed the ubiquitous presence of micronuggets of Re, which could be filtered out from the time-resolved mass spectra in most samples to expose the true amounts of Re dissolved in the silicate glass. Samples were taken after both increasing and decreasing fO$_2$ (Table 1). In addition, several time series at constant fO$_2$ were taken (Table 2). These time series demonstrate that a steady state has been reached, as is necessary for equilibrium. However, this steady state is not sufficient to prove equilibrium because of the micronugget problem. The replicate measurements in the time series after a steady state is reached can also be used to estimate the precision of the experiments (e.g., Fig. 3b,c). The effective limit of detection in our micronugget-contaminated samples

Table 2. Time series at constant fO$_2$.

Time of step (h)	Gas mix (CO:CO$_2$)	log fO$_2$	Re (ppb)	No. of samples[a]
187 + 437[b]	125:175	−8.13	309 ± 42[c]	9 (4)
314	150:150	−8.40	112 ± 7	5 (3)
665	175:125	−8.78	43 ± 4[d]	9 (7)
335	200:100	−9.05	17 ± 2[e]	5 (4)
342 + 504[b]	220:80	−9.30	10 ± 2	9 (4)
839[f]	250:50	−9.74	4.8 ± 0.5	11 (4)
336	260:40	−9.91	< 2	5
504	270:30	−10.11	< 2	7
647	280:20	−10.33	< 2	8
169	290:10	−10.61	< 2	3

[a] Numbers in parentheses are the numbers of samples from which the mean and standard deviations are computed.

[b] Crucible replenished with glass after first indicated times.

[c] See Fig. 3b.

[d] See Fig. 3c.

[e] One sample omitted with 30 ppb Re.

[f] Time includes step at CO:CO$_2$ = 240:60, which did not reach steady state.

appears to be ~2 ppb, a limit that is reached at fO$_2$ < $10^{-9.8}$ bars.

The micronugget-filtered Re solubility data correlate well with fO$_2$ as shown in Figure 4. The data at fO$_2$ ≥ $10^{-9.74}$ bars were fitted by nonlinear least squares regression to the equation:

$$[Re_{total}] = \sum_x (Q^{x+}(fO_2)^{x/4}) \qquad (1)$$

where [Re$_{total}$] is the concentration of Re in the silicate melt, x are the possible valence states of Re, and Q^{Rex+} are solubility constants to be determined in the regression. The values of Q^{Rex+} can be identified physically as the solubilities of Re^{x+} cations at the fO$_2$ of the standard state, pure O$_2$. For real experimental data with non-negligible uncertainties, the choice of which valence states (i.e., which values of x) to include in the regression cannot always be determined unambiguously by the data alone, and needs to be guided by prior chemical knowledge. The common oxidation states of Re are 4+, 6+, and 7+. We found that we could fit all the data at $10^{-7.31}$ ≤ fO$_2$ ≥ $10^{-9.74}$ bars satisfactorily assuming Re^{4+} and Re^{6+} only. The question of whether Re^{7+} may become significant at higher fO$_2$s than reached in this study will be addressed below.

We obtain Q^{Re4+} = 9.7 (±1.9) × 10^9 ppb and Q^{Re6+} = 4.2 (±0.3) × 10^{14} ppb. The data were weighted assuming an uncertainty in log fO$_2$ of 0.02, and in [Re$_{total}$] of 5% plus 2 ppb (the limit of detection). (All uncertainties, errors, etc., in this paper are reported or discussed as one standard deviation.) The value of 5% plus 2 ppb for the uncertainty in [Re$_{total}$] was estimated from a combination of the counting statistics of a typical spot analysis, the reproducibility of spot analyses from the same sample, and from different samples at the same fO$_2$ in a time-series sequence (Table 2). With this weighting, the reduced chi-squared (χ_v^2) for the 16 fitted data (Tables 1 and 2) is 1.39, indicating an excellent fit to the data at these estimated levels of experimental uncertainty. The fit and the amounts of Re^{4+} and Re^{6+} as a function of fO$_2$ are shown in Figure 4.

The crossover point at which [Re^{4+}] = [Re^{6+}] occurs at fO$_2$ = $10^{-9.3}$ bars. This oxygen fugacity is 0.4 log-bar units above the Fe-"FeO" (IW) oxygen buffer and 3.0 log-bar units below the quartz-fayalite-magnetite (QFM) buffer at 1400°C. Terrestrial magmas are usually more oxidized than this; consequently, Re dissolves in terrestrial magmas predominantly as Re^{6+}. (In this and subsequent discussions, we assume that relative redox states, as measured by differences in log fO$_2$ from common buffers like IW or QFM, can be extrapolated up or down temperatures. This is usually a good first approximation, as most condensed-phase redox equilibria plot along roughly parallel slopes in log fO$_2$ − 1/T space.) On the Moon, however, where oxygen fugacities are below IW, Re would dissolve predominantly as Re^{4+}. From this perspective, it is thus likely that the geochemical behaviour of Re may differ in the Moon and in other reduced extraterrestrial environments from its behaviour in the Earth, depending on whether there is a significant difference between the high-temperature geochemical properties of Re^{4+} and Re^{6+}. However, the total solubility of Re in silicate melt at typical lunar redox conditions is so small that the behaviour of Re is probably dominated by
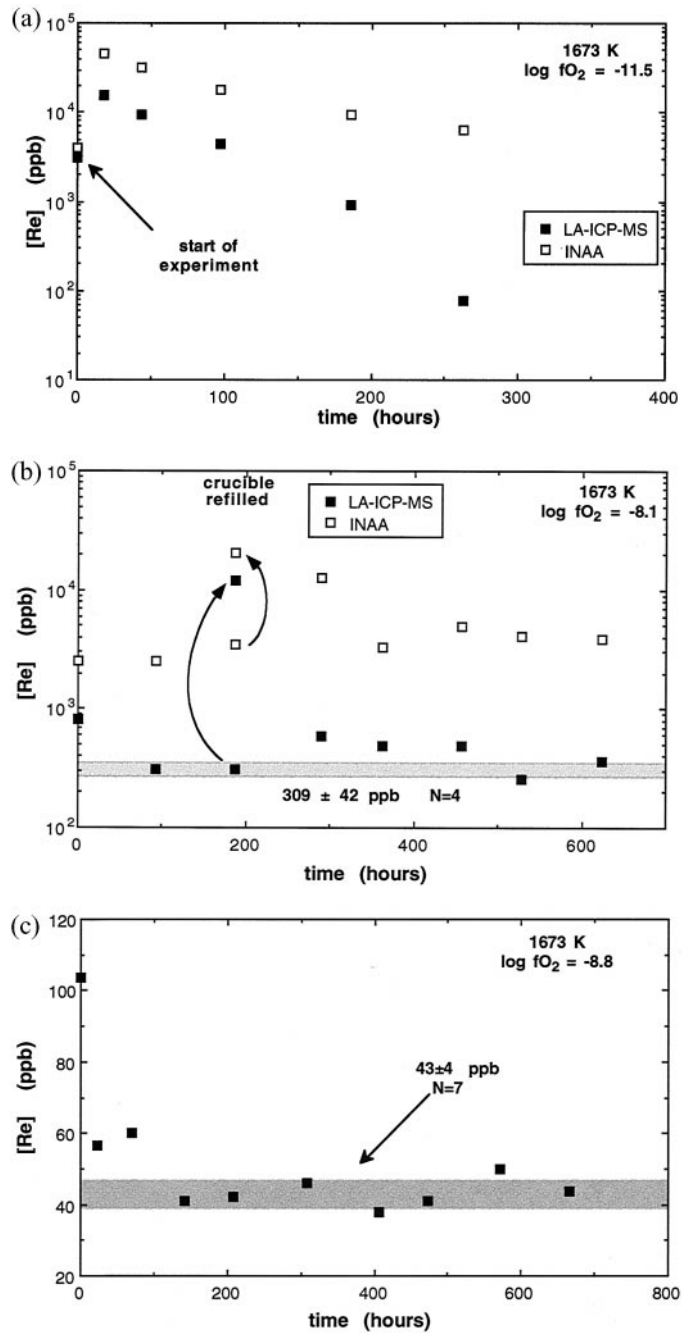
Fig. 3. Examples of time series. Re analyses by LA-ICP-MS are given by filled squares, with analyses by INAA on the same samples by open squares. The latter are thought to be compromised by suboptically sized micronuggets that have been filtered out of the former. (a) Start of the experiment. Initially, LA-ICP-MS and INAA analyses are similar. The Re levels then increase due to oxidation of the Re crucible by residual oxygen in the glass and elsewhere in the experimental apparatus. The rate at which the true Re solubility (as given by the LA-ICP-MS analyses) decreases is conspicuously faster than the rate of decrease of the micronuggets. Note that a steady state was not reached during this step. (b) This step includes replenishment of the crucible with more glass. The oxygen introduced into the experiment by this process increases Re levels (both soluble Re and micronuggets), which then decrease to the same levels as before, demonstrating reproducibility not only of the Re solubility, but also of the level of micronugget contamination. This demonstrates unambiguously that neither reaching a steady state nor reproducibility is a usable guide (let alone, proof) that measured bulk Re levels represent equilibrium solubilities. (c) Demonstrating reproducibility and precision at fairly low Re levels. The Re concentration scale in this figure is not logarithmic; hence, INAA results are not plotted.
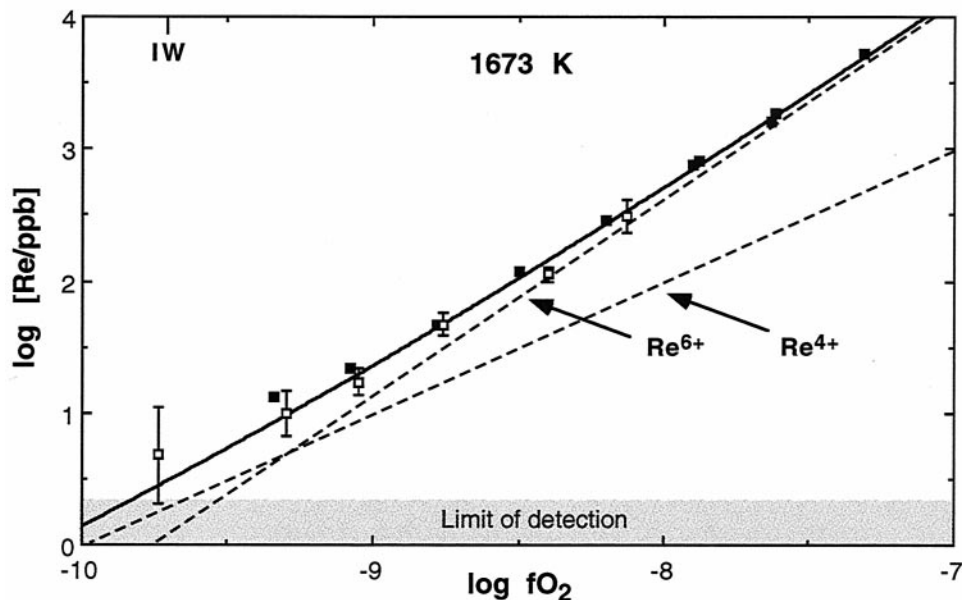
Fig. 4. Re solubilities plotted vs. log fO_2. Closed squares are individual data (Table 1), and open squares are mean values from time series with observed standard deviations as error bars (Table 2). The levels of Re^{4+} and Re^{6+} from the data fitting are plotted as dashed lines. The limit of detection (shaded area) is 2 ppb.

the presence of tiny amounts of metal, perhaps in the form of naturally occurring micronuggets.

3.2. The Micronugget Problem

Since INAA is a bulk method of analysis (mg quantities vs. ng quantities for LA-ICP-MS), it returns the total Re in the samples, from both the micronuggets and the dissolved Re. In nearly every sample, the contribution from the micronuggets overwhelms that from the dissolved Re. Nevertheless, nearly all samples contain <10 ppm Re, most <1 ppm in the way of micronuggets. That these levels predominate over the true Re solubilities is of course due to the very low Re solubilities under the experimental conditions used here, rather than any superabundance of the micronuggets. As pointed out in Ertel et al. (1999), the magnitude of the "blips" in the time-resolved LA-ICP-MS spectra indicate that the micronuggets are submicroscopic in size, being roughly the size expected of colloidal particles. And at a total concentration of ~1 ppm (i.e., 10^{-7} by volume fraction), the chances of locating them by electron microscopy would appear minimal.

To illustrate the pernicious behaviour of the micronuggets in confounding normal experimental expectations, the INAA results for two of the time series are plotted in Figure 3a,b along with the LA-ICP-MS results. Figure 3a shows the start of the experiment. The abundance of micronuggets as given by the bulk INAA results decreases towards a steady-state value with time, as does the true solubility (given by the LA-ICP-MS results). However, the rate of decrease of the micronuggets is actually much less than that of the dissolved Re. Figure 3b shows a time series, during which the crucible was replenished with starting material glass. Both the level of micronuggets and the dissolved Re increase and then return to previous levels. The amount of Re as micronuggets appears fairly constant

(although note the logarithmic scale), indicating that a steady state has been established. Thus, in these experiments steady-state conditions and even so-called reversibility are not good indicators of thermodynamic equilibrium. The present study reinforces our conclusions from previous work on the HSEs, that a systematic dependence on oxygen fugacity, plus analysis on an appropriate sampling scale, are needed to demonstrate equilibrium.

4. DISCUSSION

4.1. Comparison with Previous Work

Previously we have reported preliminary results from an earlier experiment at similar conditions of melt composition, temperature, and fO_2, which used the same experimental approach as here, except that the samples were analysed only by INAA (O'Neill et al., 1995). Because only a bulk analytical method was used, these earlier results are compromised by the micronugget effect and, therefore, do not represent true solubilities. The total Re contents are similar to those obtained by INAA in this study (Fig. 5). At the highest fO_2s, these Re values approach the true solubility curve (as obtained in this study, also shown in Fig. 5) as the contribution from dissolved Re becomes larger than that from the micronuggets.

A drawback of the experimental approach used in this study is that the experimentally accessible fO_2 range is limited to conditions more reducing than ~10^{-7} bars (at 1400°C), because of the volatility of Re as gaseous oxide species at higher fO_2 (Borisov and Jones, 1999). Righter and Drake (1997) circumvented this problem by studying the solubility of Re in equilibrium with Re-Ni alloys inside sealed silica tubes. The fO_2 of the experiments was calculated from the distribution of Ni between the alloy and melt; the activity of NiO in silicate
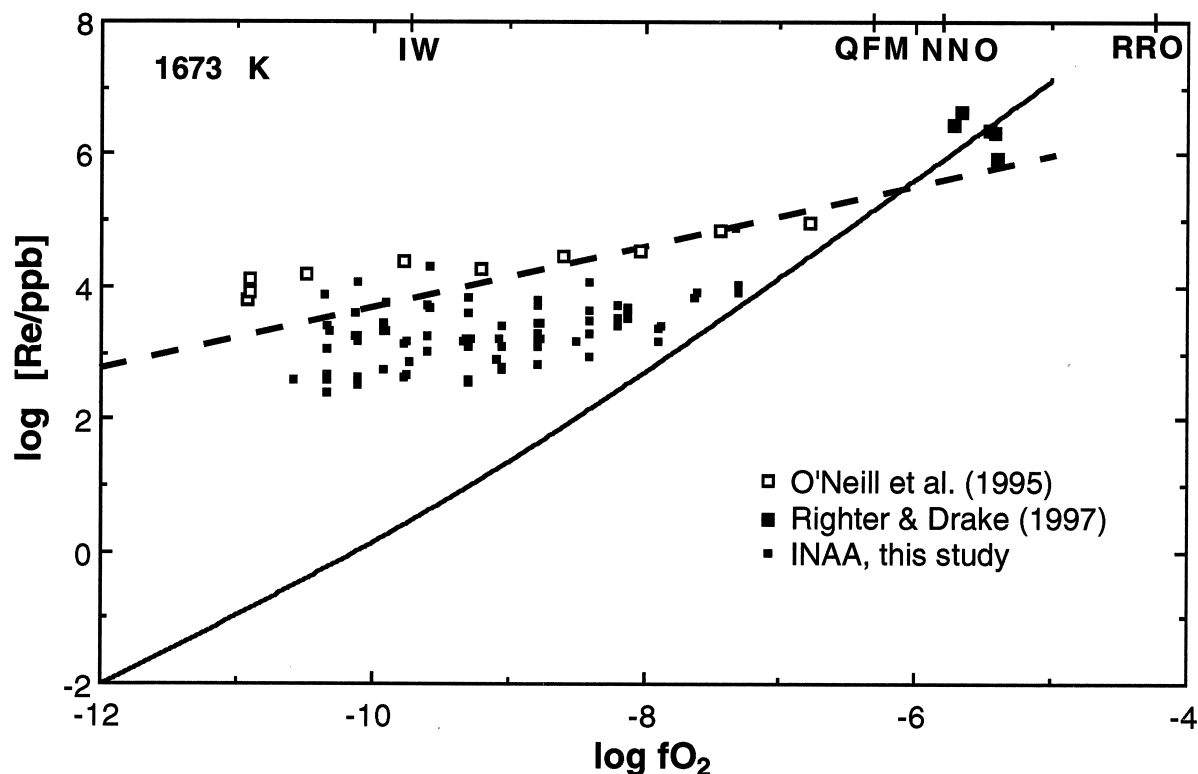
Fig. 5. Results of this study extrapolated to higher fO$_2$ compared with those of Righter and Drake (1997). Also shown are the results of the INAA bulk analyses of this study and of the similar experimental study of O'Neill et al. (1995), thought to be contaminated by micronuggets. The solid line is the best-fit solubility curve from this study (from Fig. 4) The dashed line is the Re solubility predicted from the parameterization of Righter and Drake (1997) at 1400°C and the anorthite-diopside eutectic silicate melt composition. This parameterization was in part based on the results of O'Neill et al. (1995) and is therefore in poor agreement with the true Re solubilities at low fO$_2$.

melts has been extensively studied (e.g., Holzheid et al., 1997; Ertel et al., 1997). Because the activity-composition relations of Re-Ni alloys are known, at least approximately (Okamoto 1992), these data may be adjusted to solubilities in equilibrium with pure Re metal and directly compared to the results of this study. The comparison is shown in Figure 5. (The difference in temperatures between the study of Righter and Drake, 1150–1350°C, and that of this study, 1400°C, is fairly small compared to the temperature range covered by Righter and Drake, over which no significant temperature effect is discernible, provided fO$_2$s are considered relative to the Ni-NiO buffer, i.e., rather than absolute values. This is because most high temperature redox equilibria have roughly similar slopes in fO$_2$-T space. The experimental values of fO$_2$ from Righter and Drake are plotted by using their tabulated values of Δlog fO$_2$ relative to Ni-NiO, with the value log fO$_2$ of the Ni-NiO buffer at 1400°C of -5.77 taken from O'Neill and Pownceby 1993). It may be seen that the results of Righter and Drake (1997) are in excellent agreement with a simple extrapolation of the present data. This agreement may be taken as evidence against the presence of significant Re^{7+} in the silicate melt even at these high fO$_2$s. Because of the large amounts of Re in these experiments (730–3800 ppm), the presence of micronuggets at the level found in our experiments (i.e., <100 ppm) would not affect results.

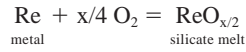Righter and Drake combined their results with the micronug-

get-contaminated, and therefore, erroneous results of O'Neill et al. (1995), along with a few high-pressure data from the literature with unknown micronugget status, to produce an equation for the partitioning of Re between silicate melt and Fe-rich metal as a function of five variables: temperature, pressure, composition of the silicate melt, sulfur content of the Fe-rich metal, and oxygen fugacity (i.e., valence state). The curve obtained from their data-fitting procedure at the conditions of this study is shown also in Figure 5. One of the effects of combining erroneous data, obtained at relatively reducing conditions with their own legitimate results from oxidizing conditions, is that the apparent valence state of Re in the silicate melt returned from the data-fitting procedure will be wrong. Thus, Righter and Drake (1997) found the effective valence state of Re to be near Re^{2+}, rather than the Re^{4+} and Re^{6+} determined here.

Based on their data fitting, Righter and Drake (1997) concluded that the metal-silicate partitioning behaviour of Re was "consistent with early equilibration between metal and silicate liquid at the base of a deep (800–1000 km) magma ocean." Clearly this conclusion can no longer be sustained. As Figure 5 shows, our new results for Re solubilities at the relevant fO$_2$ for core formation in the Earth (~IW-2) are about five orders of magnitude lower than that indicated by the earlier results reported in O'Neill et al. (1995) and the parameterization of Righter and Drake (1997) due to the micronugget problem. The

homogenous accretion scenario of Righter and Drake (1997) cannot explain the Re abundance of Earth's mantle. Rather, the Re abundance, along with those of the other HSEs, must be due to a late veneer (e.g., see review of O'Neill and Palme, 1999). This has, of course, long been advocated by students of the mantle's Re/Os isotopic systematics (e.g., Meisel et al., 1996).

4.2. Activity Coefficients of ReO$_2$ and ReO$_3$ in Silicate Melts

The solubility of each oxide component ReO$_{x/2}$ in a silicate melt may be described by the reaction:

$$\underset{\text{metal}}{Re} + x/4\ O_2 = \underset{\text{silicate melt}}{ReO_{x/2}}$$

for which, at equilibrium:

$$\ln X_{ReO_{x/2}}^{sil\ melt} = \frac{-\Delta_f G_{(ReO_{x/2})}^0}{RT} - \ln \gamma_{ReO_{x/2}}^{sil\ melt} + \frac{x}{4} \ln fO_2 \quad (2)$$

where $\Delta_f G_{(ReO_{x/2})}^0$ is the standard free energy of formation of solid ReO$_{x/2}$, $X_{ReO_{x/2}}^{sil\ melt}$ is the mole fraction of ReO$_{x/2}$ in the An-Di-eutectic silicate melt, and $\gamma_{ReO_{x/2}}^{sil\ melt}$ is the activity coefficient of ReO$_{x/2}$ in the melt, referenced to the standard state of pure solid ReO$_{x/2}$ at the temperature of interest. By substituting in Eqn. 1, one obtains:

$$\ln(k\ Q^{Re^{x+}}) = \frac{-\Delta_f G_{(ReO_{x/2})}^0}{RT} - \ln \gamma_{ReO_{x/2}}^{sil\ melt} \quad (3)$$

where k is a constant to convert the values of $Q^{Re^{x+}}$ from parts per billion to mole fractions. For the An-Di-eutectic composition melt used here, 1 ppb Re is equivalent to 2.9×10^{-10} in $X_{ReO_{x/2}}^{sil\ melt}$. Values of $\Delta_f G_{(ReO_{x/2})}^0$ may be obtained from the literature: at 1400°C, $\Delta_f G_{(ReO_2)}^0 = -135.2$ kJ mol^{-1} (Pownceby and O'Neill, 1994), and $\Delta_f G_{(ReO_3)}^0 = -155.8$ kJ mol^{-1} (extrapolated from the data in Barin, 1989). Hence, $\gamma_{ReO_2}^{sil\ melt} = 6 \times 10^3$ and $\gamma_{ReO_3}^{sil\ melt} = 0.6$ (i.e., more-or-less ideal, given the likely uncertainties). The four orders of magnitude difference in the activity coefficients is responsible for the dominance of Re^{6+} in the melt to surprisingly low fO$_2$, given the relative stabilities of the solid oxides.

This study shows that the oxidation states of Re in silicate melts, 4+ and 6+, are similar to those of Mo and W (Holzheid et al., 1994; Ertel et al., 1996). In regard to the very large value of $\gamma_{ReO_2}^{sil\ melt}$ compared to $\gamma_{ReO_3}^{sil\ melt}$, Re behaves like Mo, and not like W (Ertel et al., 1996). Re is of course recovered commercially as a byproduct from molybdenite ores, so the similarity in geochemical properties of Re and Mo in the sulfide environment is well established empirically . That this similarity should extend so well to their behaviour in silicate melts is perhaps somewhat surprising.

4.3. Estimation of Metal-Silicate Distribution Coefficients

The solubilities of Re may be converted to metal/silicate distribution coefficients using the relationship:

$$D_{Re}^{met/sil} = \frac{1}{[Re] \cdot \gamma_{Re}^{Fe,\infty}} \quad (4)$$

where $\gamma_{Re}^{Fe,\infty}$ is the activity coefficient of Re in Fe-rich metal at

infinite dilution. Unfortunately, unlike the other seven HSEs, there is no experimental information on activity coefficients of Re in Fe-rich alloys in the literature. Indeed, even the Fe-Re phase diagram is poorly known (Okamoto, 1993; Borisov and Jones, 1999; Karup-Møller and Makovicky, 1999). Righter and Drake (1997) have suggested that $\gamma_{Re}^{Fe,\infty}$ is near unity, based on a model for the systematics of binary transition metal alloys. For lack of anything more definitive, this value will be adopted here. The common observation among experimental petrologists that Fe is not lost into Re metal capsules or wire loops in experiments, except under very reducing conditions (e.g., Borisov and Jones, 1999), suggests that $\gamma_{Re}^{Fe,\infty}$ is not $\ll 1$, while the extensive mutual solid solution and the presence of intermetallic phases in the Fe-Re system guarantee that $\gamma_{Re}^{Fe,\infty}$ is not $\gg 1$. Hence the assumption of ideality for $\gamma_{Re}^{Fe,\infty}$ is probably correct within an order of magnitude. A typical basaltic, picritic, or komatiitic melt from the Earth's mantle has $a_{FeO}^{sil\ melt} \approx 0.1$, and would therefore be in equilibrium with Fe-rich metal at an oxygen fugacity 2 log-bar units below the Fe-"FeO" (iron-wüstite) oxygen buffer (IW-2), that is, at log fO$_2 = -11.7$ at 1400°C. Extrapolation of our results predicts a solubility at this fO$_2$ of 20 ppt Re (Fig. 5). This assumes that no lower oxidation state of Re becomes important at these very low fO$_2$s. We also assume that the solubility of Re in natural, Fe-containing melts is similar to that found in the Fe-free haplobasaltic melt of this study. This is clearly a major assumption that future work needs to confirm, but we note that the silicate melt compositions used by Righter and Drake (1997), whose results are compatible with ours (Fig. 5), includes two Fe-bearing compositions and contains several weight percent NiO. Then from Eqn. 4, $D_{Re}^{met/sil} = 5 \times 10^{10}$. This is considerably higher than previous estimates (e.g., Jones and Drake, 1986; O'Neill et al., 1995) and confirms that Re is indeed a highly siderophile element. However, because of the high oxidation states of Re (4+ and 6+), the solubility of Re increases rapidly with increasing fO$_2$. For example, at a typical value of fO$_2$ for the Earth's mantle of QFM-1 ($10^{-7.3}$ at 1400°C) the solubility of Re is 5.2 ppm. Furthermore, Re is not very soluble in FeS. For example, Karup-Møller and Makovicky (1999) have recently reported solubilities of Re in solid FeS of <1 wt.% in equilibrium with almost pure Re metal at 900 to 1200°C, suggesting an effective empirical value for $\gamma_{Re}^{FeS,\infty}$ of 100, referenced to pure Re metal. The sulfide/silicate distribution coefficient for Re ($D_{Re}^{sulf/sil}$) under these conditions would then only be 2×10^3. (Note that $D_{Re}^{sulf/sil}$ depends on fO$_2$ and fS$_2$; hence, this value should be viewed as illustrative only.) Thus, Re is chalcophile but not very, unlike the other HSEs. To exemplify the consequences of this, consider that the primitive mantle abundance of S is ~200 ppm, corresponding to ~0.05% sulfide. With an effective bulk rock $D_{Re}^{sulf/sil}$ of 2×10^3, half the Re would be in the sulfide, half in the silicate. Re would become even less chalcophile at higher fO$_2$ (e.g., in the subarc environment). In fact, there is increasing evidence that Re is often contained in mantle silicate phases, not sulfide (e.g., Burton et al., 1999), and that this leads to effective decoupling of Re from the other HSEs, including Os (Schmidt et al., 2000). This in turn is the fundamental reason why the Re/Os isotopic system is a good tracer of crustal influences in mantle processes in the Earth, but clearly one should not expect this geochemical principle to hold in a planet of more reduced oxidation state.

REFERENCES

Barin I. (1989) *Thermodynamic Data of Pure Substances.* VCH Verlagsgesellschaft, Weinheim, Germany.

Borisov A. and Jones J. H. (1999) An evaluation of Re, as an alternative to Pt, for the 1 bar loop technique: An experimental study at 1400°C. *Am. Mineral.* **84,** 1528–1534.

Burton K. W., Schiano P., Birck J. L., and Allègre C. J. (1999) Osmium isotope disequilibrium between mantle minerals in a spinel-lherzolite. *Earth Planet. Sci. Lett.* **172,** 311–322.

Dingwell D. B., O'Neill H. St. C., Ertel W., and Spettel B. (1994) The solubility and oxidation state of nickel in silicate melt at low oxygen fugacities: Results using a mechanically assisted equilibrium technique. *Geochim. Cosmochim. Acta* **58,** 1967–1974.

Ertel W., Dingwell D. B., and O'Neill H. St. C. (1996) Solubility of tungsten in a haplobasaltic melt as function of temperature and oxygen fugacity. *Geochim. Cosmochim. Acta* **60,** 1171–1180.

Ertel W., Dingwell D. B., and O'Neill H. St. C. (1997) Composition dependence of the activity of Ni in Silicate melts. *Geochim. Cosmochim. Acta* **61,** 4707–4721.

Ertel W., O'Neill H. St. C., Sylvester P. J., and Dingwell D. B. (1999) Solubilities of Pt and Rh in a haplobasaltic melt at 1300°C. *Geochim. Cosmochim. Acta* **63,** 2439–2449.

Hamilton D. L. and Henderson C. M. B. (1968) The preparation of silicate compositions by a gelling method. *Mineral. Mag.* **36,** 832–838.

Holzheid A., Borisov A., and Palme H. (1994) The effect of oxygen fugacity and temperature on solubilities of nickel, cobalt and molybdenum in silicate melts. *Geochim. Cosmochim. Acta* **58,** 1975–1981.

Holzheid A., Palme H., and Chakraborty S. (1997) The activities of NiO, CoO and FeO in silicate melts. *Chem. Geol.* **139,** 21–38.

Jones J. H. and Drake M. J. (1986) Geochemical constraints on core formation in the Earth. *Nature* **322,** 221–228.

Karup-Møller K. and Makovicky E. (1999) The phase system Fe-Re-S at 1200°, 1100°, 1000°, and 900°C. *Neus Jb. Miner. Monat.* (or Mh.), 265–280.

Meisel T., Walker R. J., and Morgan J. W. (1996) The osmium isotopic content of the Earth's primitive upper mantle. *Nature* **383,** 517–520.

Mendybaev R. A., Beckett J. R., Stolper E., and Grossman L. (1998) Measurement of oxygen fugacities under reducing conditions: Non-Nernstian behavior of Y_2O_3-doped zirconia oxygen sensors. *Geochim. Cosmochim. Acta* **62,** 3131–3139.

Okamoto H. (1992) Ni-Re (Nickel-Rhenium). *J. Phase Equilib.* **13,** 335.

Okamoto H. (1993) Fe-Re (Iron-Rhenium). In *Phase Diagrams of Binary Iron Alloys* (ed. H. Okamoto) ASM International, Materials Park, Ohio.

O'Neill H. St. C. and Pownceby M. I. (1993) Thermodynamic data from redox reactions at high temperatures. I. An experimental and theoretical assessment of the electrochemical method using stabilized zirconia electrolytes, with revised values for the Fe-"FeO," Co-CoO, Ni-NiO and Cu-Cu_2O oxygen buffers, and new data for the W-WO_2 buffer. *Contrib. Mineral. Petr.* **114,** 296–314.

O'Neill H. St. C., Dingwell D. B., Borisov A., Spettel B., and Palme H. (1995) Experimental petrochemistry of some highly siderophile elements at high temperatures, and some implications for core formation and the mantle's early history. *Chem. Geol.* **120,** 255–273.

O'Neill H. St. C. and Palme H. (1999) Composition of the silicate Earth: Implications for accretion and core formation. In *The Earth's Mantle: Composition, Structure and Evolution* (ed. I. Jackson), pp. 3–126, Cambridge University Press, Cambridge, UK.

Pouchou J. L. and Pichoir F. (1984) A new model for quantitative X-ray microanalysis. Part 1: Applications—the analysis of homogeneous samples. *Rech. Aerospatiale* **3,** 13–38.

Pownceby M. I. and O'Neill H. St. C. (1994) Thermodynamic data from redox reactions at high temperatures. IV. The Re-ReO_2 oxygen buffer: An experimental calibration using emf and hydrothermal methods. *Contrib. Mineral. Petr.* **118,** 130–137.

Righter K. and Drake M. J. (1997) Metal-silicate equilibrium in a homogenously accreting earth: New results for Re. *Earth Planet. Sci. Lett.* **146,** 541–553.

Schmidt G., Palme H., Kratz K. L., and Kurat G. (2000) Are highly siderophile elements (PGE, Re and Au) fractionated in the upper mantle of the Earth? New results on peridotites from Zabargad. *Chem. Geol.* **163,** 167–188.

Sylvester P. J. and Eggins S. M. (1997) Analysis of Re, Au, Pd, Pt and Rh in NIST glass certified reference materials and natural basalt glasses by laser ablation ICP-MS. *Geostandard. Newslett.* **21,** 215–228.